Available online at www.sciencedirect.com
ScienceDirect
Journal of Theoretical Biology 252 (2008) 109–122
Journal of Theoretical Biology
www.elsevier.com/locate/yjtbi

Modeling of cancer virotherapy with recombinant measles viruses

Željko Bajzer[a,*], Thomas Carr[b], Krešimir Josić[c], Stephen J. Russell[d], David Dingli[e]

[a]*Biomathematics Resource and Department of Biochemistry and Molecular Biology, Mayo Clinic College of Medicine, Guggenheim 1611b, Rochester, MN 55905, USA*
[b]*Molecular Medicine Program, Mayo Clinic College of Medicine, Rochester, MN 55905, USA*
[c]*Department of Mathematics, Southern Methodist University, Dallas, TX 75275, USA*
[d]*Department of Mathematics, University of Houston, Houston, TX 77204-3008, USA*
[e]*Department of Hematology, Mayo Clinic College of Medicine, Rochester, MN 55905, USA*

Received 1 October 2007; received in revised form 16 January 2008; accepted 17 January 2008
Available online 1 February 2008

Abstract

The Edmonston vaccine strain of measles virus has potent and selective activity against a wide range of tumors. Tumor cells infected by this virus or genetically modified strains express viral proteins that allow them to fuse with neighboring cells to form syncytia that ultimately die. Moreover, infected cells may produce new virus particles that proceed to infect additional tumor cells. We present a model of tumor and virus interactions based on established biology and with proper accounting of the free virus population. The range of model parameters is estimated by fitting to available experimental data. The stability of equilibrium states corresponding to complete tumor eradication, therapy failure and partial tumor reduction is discussed. We use numerical simulations to explore conditions for which the model predicts successful therapy and tumor eradication. The model exhibits damped, as well as stable oscillations in a range of parameter values. These oscillatory states are organized by a Hopf bifurcation.

Keywords: Tumor growth modeling; Cancer therapy; Population dynamics; Oscillatory dynamical systems

1. Introduction

Many neoplasms remain incurable despite the introduction of novel therapies. In response to the demand for novel cancer therapeutics, replication competent vectors (both DNA and RNA based) have been introduced as potential cancer therapy agents (Kirn et al., 2001; Russell, 2002). Replication selective adenoviruses have been tested in several trials for head and neck cancer (Nemunaitis et al., 2001) as well as metastatic colon carcinoma (Reid et al., 2001, 2002), while Newcastle disease virus has been given to patients with various tumor types (Pecora et al., 2002). An underlying premise of tumor virotherapy is that the infected tumor cells become factories that generate new virus particles which proceed to infect additional tumor cells in a series of waves (Kirn et al., 2001). The outcome of therapy depends in a complex way on the interactions between the population of virus and tumor cells. Several attempts have been made to understand and characterize this dynamical system by mathematical models (Wodarz, 2001, 2003; Wu et al., 2001, 2004; Wein et al., 2003; Tao and Guo, 2005; Dingli et al., 2006a; Friedman et al., 2006). It remains essential to validate those models by appropriate experimental observations and data.

Our experimental work has centered on the use of vectors derived from the Edmonston vaccine strain of measles virus (MV-Edm). These vectors have potent and selective oncolytic activity against a wide variety of human tumors including non-Hodgkin lymphoma (Grote et al., 2001), multiple myeloma (Peng et al., 2001), ovarian carcinoma (Peng et al., 2002b), cerebral glioma (Phuong et al., 2003) and breast carcinoma (McDonald et al., 2006) without any harmful effects on normal tissues. This tumor selectivity is partly dependent on high-level expression of CD46 by tumor cells (Anderson et al., 2004; Ong et al., 2006), the receptor preferentially used by these vectors for entry into cells (Schneider et al., 2002). In addition, protein

*Corresponding author. Tel.: +1 507 284 8584; fax: +1 507 284 2053.
E-mail address: bajzer@mayo.edu (Ž. Bajzer).

0022-5193/$ - see front matter © 2008 Elsevier Ltd. All rights reserved.
doi:10.1016/j.jtbi.2008.01.016

engineering has enabled the production of fully re-targeted viruses that only infect the tumor cells of interest (Nakamura et al., 2004, 2005; Hadac et al., 2004). Furthermore, MV vectors have been engineered to enable the secretion of biologically inert soluble peptides such as carcinoembryonic antigen (CEA, MV-CEA) and human chorionic gonadotrophin from infected cells (hCG, MV-hCG) (Peng et al., 2002a) so that viral gene expression can be serially followed non-invasively in vivo. MV-Edm has also been modified to induce expression of the thyroidal sodium iodide symporter (NIS, MV-NIS) in infected cells that allows in vivo, non-invasive imaging of the biodistribution and replication of the virus while also enhancing the oncolytic effect when virotherapy is combined with radioactive iodide isotopes (Dingli et al., 2004, 2006b). These developments will enrich the experimental basis necessary for adequate modeling, which in turn can help understanding and prediction of virotherapy outcomes.

Infection by MV starts when the viral hemagglutinin (H) protein interacts with its receptor (CD46) on target cells. This interaction triggers conformational changes in the viral fusion (F) protein that leads to fusion of the viral and cell plasma membranes, allowing the viral nucleoprotein complex to enter into the cell. Infected cells start to express the viral H and F proteins on their own plasma membrane. The H protein interacts with CD46 on neighboring cells and can trigger membrane fusion between cells leading to fusion of the two cells together. As the expression of the viral H and F proteins increases, the probability that an infected cell fuses with a neighboring tumor cell increases. Once two cells fuse, there is an effective decrease in the concentration of viral proteins expressed on the cell surfaces and therefore there is a delay in spread of fusion until additional proteins are expressed on the surface. In time, this spread of cell-to-cell fusion leads to the formation of giant cell syncytia that normally die after a few days (Peng et al., 2001, 2002b). Infected cells that have been incorporated into syncytia stop replicating and do not contribute to further growth of the tumor population. In addition, once infected cells die, they might release free virus particles that can infect surrounding cells.

Although MV based vectors have potent oncolytic activity, some tumors are not eliminated in vivo. Studies using MV-CEA show that although the virus efficiently infects and propagates in these tumors, the latter may persist (Peng et al., 2002b, 2006; Dingli et al., 2004). This highlights the dynamic interplay between viral replication, tumor cell growth and the death rate of infected tumor cells (Wodarz, 2001, 2003; Wu et al., 2001, 2004; Wein et al., 2003; Tao and Guo, 2005; Dingli et al., 2006a; Friedman et al., 2006). In our prior mathematical analysis of MV based tumor therapy, we did not consider the impact of cell-to-cell fusion (Dingli et al., 2006a). Moreover, in that analysis, we followed the path of Wodarz (2003) and did not compensate for the fact that virus particles which have infected cells are not available to infect additional cells, leading to a potential imbalance in the model. The goal of this paper is to derive, validate and analyze a more biologically coherent model that takes both of these considerations into account. The model allows us to study the impact of both cell-to-cell fusion as well as the efficiency of virus infection of tumor cells on the outcome of therapy. We validate the proposed model by using tumor growth data from in vivo experiments in which human myeloma tumor xenografts were grown in immunodeficient mice (Dingli et al., 2004). Since the mice that harbored the tumors could not mount an immune response to viral antigens, the described model does not explicitly take the immune response into account.

The paper is organized as follows: In the next section we derive our model for virotherapy and discuss previously proposed models. In Section 3 we determine equilibria of the model corresponding to therapy success, therapy failure and partial-therapy success, and discuss their stability. Following that, in Section 4, we validate the model and determine probable values of model parameters by fitting to experimental data. By using simulations in Section 5 we explore the predictions of the model for successful therapy outcome and for oscillatory behavior. We briefly summarize and discuss our findings in Section 6.

2. Mathematical models

Within the framework of modeling interacting populations by systems of ordinary differential equations, Wodarz (2001) and Wodarz and Komarova (2005) proposed the following model:

$$y' = \bar{r}y[1-(x+y)/C] - dy - \beta xy, \tag{1}$$

$$x' = \beta xy + sx[1-(x+y)/C] - ax. \tag{2}$$

The term $\bar{r}y[1-(x+y)/C]$ in (1) describes the logistic growth rate of an uninfected tumor cell population $y(t)$, and the analogous term $sx[1-(x+y)/C]$ in (2) represents the growth rate of the virus infected cell population $x(t)$. Constants $\bar{r}>0$ and $s>0$ are the respective growth rate constants, while C is the carrying capacity or maximal tumor size so that $x+y\leqslant C$. The term βxy represents the infection rate, with β being the rate constant. When an infected cell interacts with an uninfected cell, then the latter also becomes infected. The term dy represents the death rate of uninfected cells, and ax represents the death rate of infected cells as a consequence of virus infection.

This model does not include a population of free virus particles; infection by free virus and the release of virions by infected cells are only indirectly modeled by the rate constant β that somehow captures virus production. Some in vivo experiments (Peng et al., 2002a, 2006) suggest that free measles virus particles are not detectable, yet this could be important in modeling transient effects of initial infection by the virus. In a more recent paper Wodarz (2003) introduced a free virus population, and removed the growth term for infected cells. Indeed, there is experimental

evidence that several different viruses inhibit cellular replication after infection (Heaney et al., 2002). The proposed model takes the form (Wodarz, 2003)

$$y' = \bar{r}y[1-(x+y)/C] - dy - \kappa yv, \tag{3}$$

$$x' = \kappa yv - (d+a)x, \tag{4}$$

$$v' = \alpha x - \omega v. \tag{5}$$

Here the new term κyv models the spread of infection in tumor cells by a productive encounter of one free virus particle with an uninfected cell. Thus, κyv represents the rate of infection of uninfected cells by free virus $v(t)$, with $\kappa > 0$ being the corresponding rate constant. In this model, the death rate constant $d+a$ of infected cells consists of the death rate of uninfected tumor cells (d) and the death rate caused by virus (a). The term αx models the release of virions by infected cells with the rate constant α, and ωv is the rate of elimination of free virus particles by various causes including non-specific binding and generation of defective interfering particles. In our earlier work we have further modified the above model by introducing a more realistic growth term for uninfected tumor cells (Dingli et al., 2006a). It is known that untreated tumor growth is reliably described by the Gompertz model (Marušić et al., 1994; Bajzer et al., 1997; Cameron et al., 2001; Chignola et al., 2000), or for some tumors by the more general Bertalanffy–Richards (BR) (or generalized logistic) growth model (Spratt et al., 1993), which can be written in the form

$$y' = (g/\varepsilon)y[1-y^{\varepsilon}/K^{\varepsilon}], \quad \varepsilon > 0. \tag{6}$$

In the limit $\varepsilon \to 0$ this model becomes the Gompertz model (Byrne, 2003; Bajzer et al., 1996), and thus can be considered sufficiently general. The proposed model of virotherapy (Dingli et al., 2006a) is therefore

$$y' = ry[1-(y+x)^{\varepsilon}/K^{\varepsilon}] - \kappa yv, \tag{7}$$

$$x' = \kappa yv - \delta x, \tag{8}$$

$$v' = \alpha x - \omega v. \tag{9}$$

Compared to Eq. (3), in Eq. (7) we have omitted the term dy because it is redundant (Dingli et al., 2006a). Namely, the equation $y' = \bar{r}y[1-(y+x)^{\varepsilon}/C^{\varepsilon}] - dy - \kappa yv$ is equivalent to (7) if we define the parameters as $r = \bar{r} - d$, $K = (1-d/\bar{r})^{1/\varepsilon}C$. Similarly, the death rate $(d+a)x$ in (4) can be represented by δx. The rate constant δ could also model some effects of the immune system, provided that the elimination of the infected cells by immune response is approximately proportional to the size of the infected cell population. In addition, if there is any low level of proliferation of infected cells, it can be effectively taken into account by $\delta > 0$, which then consists of four terms: $\delta = d + a + d_i - r_x$, where d_i models effects of the immune response and r_x models possible small proliferation rate constant.

Close inspection of the model (7)–(9) reveals that it is still deficient on two accounts:

1. It is missing a term which describes infection from an encounter between an infected cell(s) (expressing viral F and H proteins) and an uninfected cell resulting in cell fusion that produces a syncytium. The resulting syncytium can fuse with other uninfected cells. Experimental evidence suggests that the intratumoral spread of infection occurs mostly due to such fusion between infected and uninfected cells, rather than by free virus infection (Peng et al., 2002b; Dingli et al., 2004).
2. Eq. (9) is missing the term $-\kappa yv$ which represents the elimination of free virus particles and could be important (see Section 3). We assume that one virus particle infects one cell. Once a virus enters a cell, it is incapable of infecting additional cells and ceases to be part of the free virus population. It is unlikely that syncytia release free virus particles when they die, since syncytial death occurs by apoptosis that destroys the cell from within. It is interesting to note that a more complex, and possibly more realistic, spatio-temporal models proposed in Wu et al. (2001, 2004), Wein et al. (2003), Tao and Guo (2005), Friedman et al. (2006) also do not include the term analogous to $-\kappa yv$ in the equation for the rate of change of virus population.

When these two missing terms are introduced, the model we propose and analyze in the present work is given by

$$y' = ry[1-(y+x)^{\varepsilon}/K^{\varepsilon}] - \kappa yv - \rho xy, \tag{10}$$

$$x' = \kappa yv - \delta x, \tag{11}$$

$$v' = \alpha x - \omega v - \kappa yv, \tag{12}$$

and is represented diagrammatically in Fig. 1. The parameter $\rho > 0$ is the rate constant describing cell-to-cell fusion with the formation of syncytia. In this model $x(t)$ represents the population of both single infected cells and syncytia. Both die at an effective rate constant $\delta > 0$. The term ρxy does not appear in Eq. (11) because no new

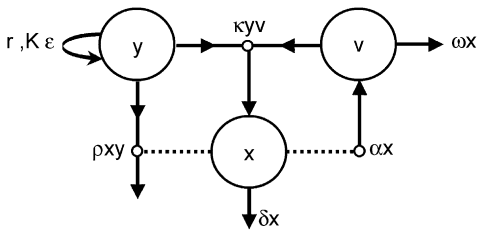

Fig. 1. Schematic diagram of the proposed model for virotherapy. Here y denotes the populations of uninfected cells. Proliferation of these cells is described by an effective proliferation rate r, carrying capacity K and parameter ε which characterizes the shape of the sigmoidal growth curve. Populations of infected cells and virus are denoted by x and v, respectively. Indicated rates of first and second order are explained in Table 1. Solid line arrows signify population influx or depletion, while dotted lines indicate that corresponding rates depend on population x.

members are added to population $x(t)$ when an uninfected cell is incorporated into a syncytium by cell-to-cell fusion. This term is therefore conceptually different from the term βxy in (1) and (2). We summarize the parameters in Table 1 for ease of reference. As in the model given by Eqs. (7)–(9), the tumor burden $u(t) = x(t) + y(t)$ cannot exceed the carrying capacity K. The proof is analogous to the proof given in Appendix A of Dingli et al. (2006a).

We denote the initial tumor burden by $y(0) = y_0$, and assume that at time $t = 0$ a population $v(0) = v_0$ of virus particles is introduced. The initial population of infected cells is $x(0) = 0$. The model parameters were determined by fitting the model (10)–(12) to available data for tumor size as a function of time (see Section 4). Tumor size was measured as volume (in mm^3), while our model considers population of cells. We convert tumor volume to cell population by assuming $1\,mm^3$ corresponds to 10^6 cells, and in what follows, we consider cell and virus populations y, x, v as expressed in units of 10^6. Throughout the paper we assume that all time units are expressed in days.

The goal of cancer virotherapy is to eliminate tumor cells. Within the context of our model, we can assume that the tumor is completely eliminated when the total population of tumor cells is reduced to one cell, which means that in our adopted units $u(t) = x(t) + y(t) = 10^{-6}$. In general, deterministic population dynamics models such as (10)–(12) and models considered in Wodarz (2001, 2003), Wu et al. (2001, 2004), Dingli et al. (2006a), Tao and Guo (2005), and Wein et al. (2003) may not be realistic when the sizes of interacting populations are very small, so in some ways the lowest limit of 1 cell is artificial. Yet, it may be considered as a relatively conservative estimate of tumor eradication. Obviously, $u(t) = 10^{-6}$ should be achieved at some finite time $t = t_e \leqslant T$, where T is the estimated maximal lifetime of the host organism. We will assume $T = 1000$ days for a mouse. If the average tumor burden is diminishing and at time T it has decreased to the size which is below the limit of detectability, we consider therapy to have been successful. In general, a population of 10^6 cells growing under the skin is not detectable clinically. Thus, if $u(T) \leqslant 1$ (in adopted units) we consider therapy successful, although the tumor is not completely eliminated.

Table 1
Parameters and corresponding units used in the present model (10)–(12)

r	Effective growth rate of uninfected cells (day^{-1})
K	Carrying capacity (in 10^6 cells)
κ	Infection rate constant (per day per 10^6 cells or virions)
ρ	Rate constant of cell fusion (per day per 10^6 cells)
δ	Effective death rate constant of infected cells (day^{-1})
ω	Rate constant of virus elimination (day^{-1})
α	Virus production rate constant by infected cells (virions per day per cell)

3. Analysis of equilibria

In the absence of more complex attractors, the outcome of virotherapy can be characterized by the stable states of the system (10)–(12), unless the tumor burden $u(t)$ has been reduced to a level below 1 cell ($u(t) < 10^{-6}$) at some finite time. We therefore begin by discussing the stability of the three possible equilibria of the model listed in Table 2.

3.1. Stability of equilibria

The desired outcome of therapy corresponds to the equilibrium at the origin (the first equilibrium in Table 2). As the corresponding eigenvalues indicate, this point is unstable for biologically relevant parameters. The unstable manifold of this equilibrium is the y-axis. The instability of the equilibrium is due to the fact that in the absence of the virus, the number of infected cells x will remain at 0, and all solutions will remain on the y-axis. In this case uninfected cells y will exhibit growth according to the BR model and move away from the origin.

Equilibrium 2 represents failure of virotherapy, as the tumor attains its maximal size K. The stability of the point is determined by eigenvalue λ_2, as the real parts of the remaining eigenvalues are negative. In particular, the stability of the point is determined by q (defined in Table 2): when $q < 0$ the equilibrium is stable, while it is unstable for $q > 0$. We will see next that this equilibrium undergoes a bifurcation when $q = 0$.

Partial success of virotherapy is represented by the third equilibrium. Since, $x(t) + y(t) \leqslant K$, this equilibrium point can be reached only if $y_3 \leqslant K$. Although this equilibrium is defined implicitly, one can show that for biologically relevant parameters (positive rate constants), and when $\alpha > \delta$, this equilibrium point exists and is unique (the proof is analogous to the proof presented in Appendix C of Dingli et al., 2006a). If stable, equilibrium 3 implies that a permanent reduction of tumor burden can be reached, even if virotherapy is not completely successful.

Note that when $y_3 = K$, the equation for x_3 is only satisfied for $x_3 = 0$, also implying that $v_3 = 0$. Therefore,

Table 2
Equilibria of system (10)–(12) and their associated eigenvalues

Equilibrium	Eigenvalues
$y_1 = 0$ $x_1 = 0$ $v_1 = 0$	$\lambda_1 = r > 0$ $\lambda_2 = -\delta < 0$ $\lambda_3 = -\omega < 0$
$y_2 = K$ $x_2 = 0$ $v_2 = 0$	$\lambda_1 = -r\varepsilon < 0$ $\lambda_2 = -A + \sqrt{A^2 + q}$ $\lambda_3 = -A - \sqrt{A^2 + q}$ $A = (\omega + \kappa K + \delta)/2, \quad q = (\alpha - \delta)\kappa K - \delta\omega$
$y_3 = \delta\omega/[\kappa(\alpha - \delta)]$ $x_3 = c[1 - (x_3 + y_3)^{\varepsilon}/K^{\varepsilon}]$ $v_3 = (\alpha - \delta)/\omega x_3$ $c = r\omega/[(\alpha - \delta)\kappa + \rho\omega]$	See discussion

when the parameters satisfy

$$\delta\omega = (\alpha - \delta)\kappa K \tag{13}$$

equilibrium points 2 and 3 coincide. In fact this collision occurs precisely when $q = 0$, that is, when equilibrium 2 is expected to undergo a bifurcation. It can be shown that this is typically a transcritical bifurcation, in which equilibrium 2 and 3 exchange stability. More precisely, as the parameters are changed, equilibrium 3 enters the positive orthant by passing through equilibrium 2. In the collision, the eigenvalue λ_2 becomes positive, while one of the eigenvalues of equilibrium 3 becomes negative.

A direct computation shows that if Eq. (13) is satisfied and if κ or α are increased, or ω is decreased, then the transcritical bifurcation will result in equilibrium 3 being in the positive orthant. This agrees with intuition, since an increase in infection rate or virus production, or a decrease in the rate of virus elimination should increase the effectiveness of therapy. The dependence on the parameter δ can be determined similarly: If $\omega < \kappa$, then a decrease in δ from its bifurcation value leads to the entrance of equilibrium 3 into the positive orthant.

The eigenvalues of equilibrium 3 are not analytically tractable in general. However, in Section 5 we show that this equilibrium can undergo a Hopf bifurcation such that the cell and virus populations oscillate in time.

3.2. Equilibria in a singular model

In the next section we show that the experimental data for myeloma in mice under virotherapy with MV-NIS are consistent with $\alpha = \omega = 0$. This singular model implies that no free virus is being produced in vivo, and that the size of free virus population is not decreased by elimination or inactivation. In this case equilibrium 1, corresponding to successful therapy, and equilibrium 2, corresponding to therapy failure, remain unchanged in location and stability.

In addition there is a line of fixed points given by

$$L = \{(y, x, v) : y_3 = x_3 = 0 \text{ and } v = \overline{v} \text{ arbitrary}\}. \tag{14}$$

These equilibria represent the situation when the tumor is eradicated, but there is a residual virus population $\overline{v}$. The size of this residual population depends on initial conditions, since the virus population remaining is from the initial dose injected for therapy. The Jacobian at each of these equilibria has the eigenvalues

$$\lambda_1 = 0, \quad \lambda_2 = -\delta < 0, \quad \lambda_3 = r - \kappa\overline{v}. \tag{15}$$

The eigenvalue λ_1 corresponds to an eigenvector parallel with L, and the stability of points on L is determined by the sign of λ_2 and λ_3. Therefore all points satisfying

$$\overline{v} < \frac{r}{\kappa} \tag{16}$$

are stable, and collectively form an attractor L^A. The points satisfying the opposite inequality are unstable. As shown in Fig. 2 the point $(0, 0, r/\kappa)$ lies on a separatrix between the basin of attraction of L^A, and the basin of attraction of the equilibrium $(K, 0, 0)$ representing therapeutic failure (this equilibrium is not depicted in Fig. 2, as it lies on y-axis far above the maximal ordinate of 10).

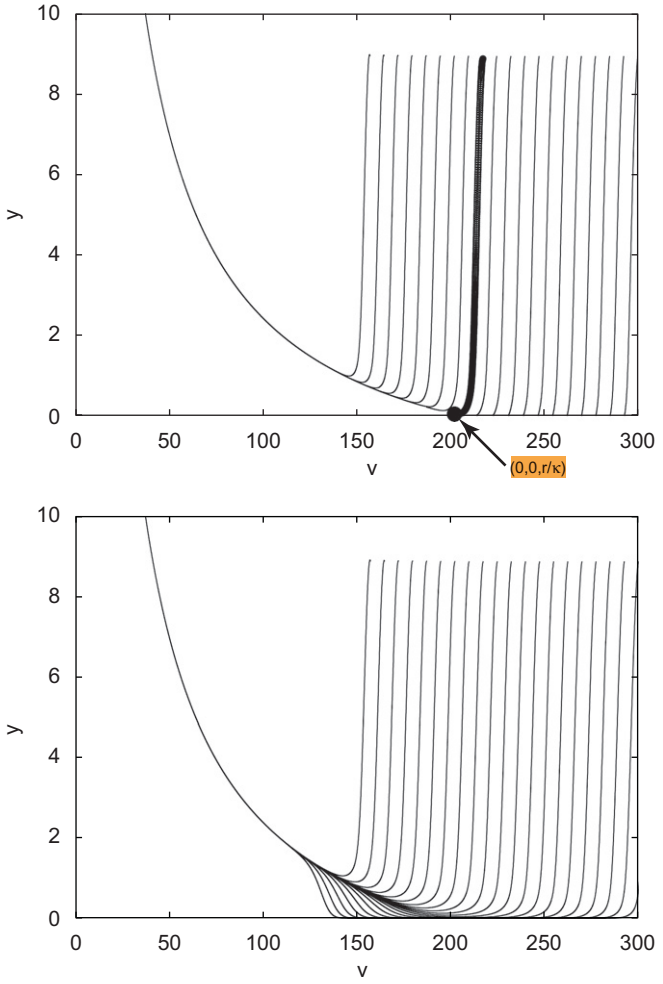

Fig. 2. Top: the projection onto the v–y plane of a collection of orbits in the singular case $\alpha = \omega = 0$. Initial values $v(0)$ range between 155 and 305, $y(0) = 9$, and $x(0) = 0$. The orbit singled out by the heavy line lies on the separatrix between two basins of attraction. Points to the left are attracted to the equilibrium $(K, 0, 0)$ (therapeutic failure), and points to the right are attracted to the line of fixed points L (successful therapy). Other parameters are chosen as $r = 0.206, \rho = 0.2145, K = 2139, \varepsilon = 1.649, \kappa = 0.001$, $\delta = 0.5115$. Bottom: the same simulation with $\alpha = \omega = 0.001$. The line L is no longer attracting.

Note that the line L is invariant for all parameter values. However, when α and ω are small and positive, which still might be consistent with our data (see Section 4), then L is no longer attracting.

Finally, Fig. 3 shows the specific trajectories in the full 3-D phase space such that $x(1000) + y(1000) = u(1000) = 1$, the minimum size for a detectable tumor at $t = 1000$. The $(y, 0, v)$ plane is gray scale coded according to the size of the tumor at $t = 1000$, the natural lifetime of the mouse. Initial conditions such that the point $(y, 0, v)$ is light lead to $u(1000) > 1$, while points where $(y, 0, v)$ is dark corresponds to $u(1000) < 1$ which may imply successful therapy or even complete tumor elimination. The black line in the $(y, 0, v)$

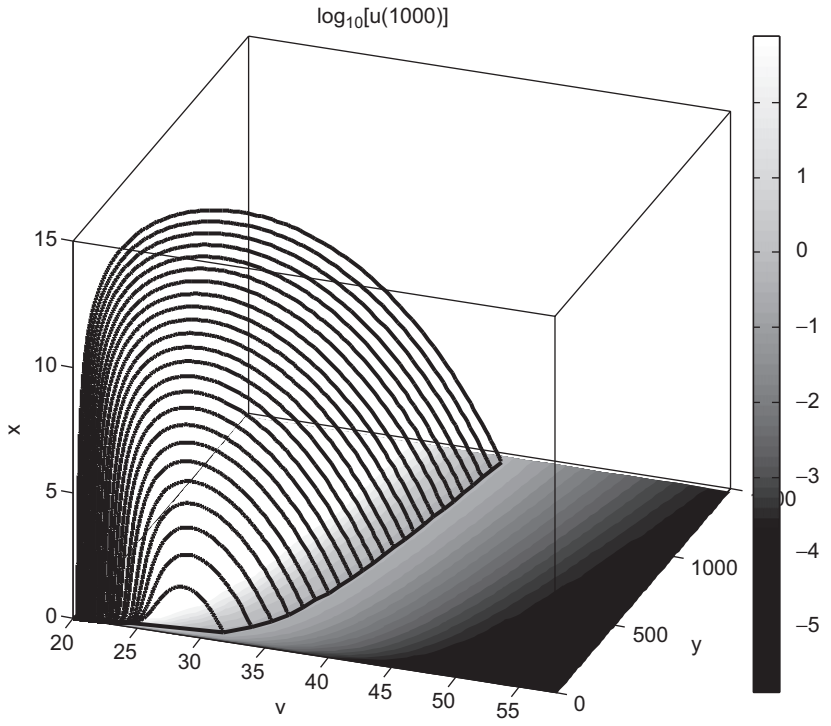

Fig. 3. Initial conditions $(y, 0, v)$ for the initial tumor size and virus population are gray scale coded by the total tumor size $u = y + x$ at $t = 1000$. The family of depicted trajectories all emanate from initial conditions such that $u(1000) = 1$, which defines the threshold for successful therapy. Parameter values are $r = 0.0206$ (0.1 times the value of r in Fig. 2), $K = 2139, \varepsilon = 1.649$, with other parameters take from fit (a) in Table 3.

plane is the boundary between these two conditions. For a fixed initial tumor size y, the curve defines the minimum value of initial virus dose that is necessary for successful therapy. The family of trajectories defines a surface such that all initial conditions whose trajectories are above the surface will lead to successful therapy, $u(1000) < 1$; conversely, all initial conditions whose trajectories are below the surface will lead to $u(1000) > 1$. Thus, for a fixed initial tumor size y, we see that successful therapies require a greater initial dose of virus v, and lead to a greater number of infected tumor cells x, before the complete tumor $u = y + x$ is eradicated.

4. Model validation and parameter estimation

Experimental data for multiple myeloma xenografts grown in SCID mice (Dingli et al., 2004) were used to validate the proposed model (10)–(12). These data included the untreated tumor growth curve and the growth curve when virotherapy is introduced on day 15. Tumor size was measured as volume in mm^3, while our model considers population of cells. As mentioned in Section 2 we assume that $1\,mm^3$ corresponds to 10^6 cells, and consequently consider cell and virus populations y, x, v as expressed in units of 10^6.

The model was validated and parameters estimated by using the weighted non-linear least-squares method. Weighting factors were chosen as $1/\sigma_i^2$, where σ_i is the experimentally determined standard deviation for the ith data point (see Fig. 4). We performed the least-squares fitting by using the Simplex-Induction Hybrid minimizer (Offord and Bajzer, 2006) in conjunction with a custom coded ODE solver.

Growth curve data for untreated tumor were fitted (Dingli et al., 2006a) by using the Gompertz, logistic (L) and BR models (Byrne, 2003; Bajzer et al., 1996; Marušić et al., 1994). The Gompertz model did not fit well (Dingli et al., 2006a), the logistic model fitted fairly well (see Fig. 4; curve designated with L) and the BR model with $\varepsilon \approx 1.65$ provided the best fit (Fig. 4, curve designated with BR) as determined by model selection criteria (Dingli et al., 2006a).

The values for parameters r, K, ε, were obtained by fitting the BR model to growth data for untreated tumors, and then used in fitting virotherapy data (full squares in Fig. 4). The tumor size y_0 at the beginning of virotherapy (day 15 after tumor inoculation) was obtained from the best-fit curve by BR model, and the initial viral dose v_0 was experimentally known. The minimization was then performed with respect to parameters $\kappa, \rho, \delta, \alpha$ and ω. The best fit was obtained when the lower limit for the allowed values of parameters α and ω was set to zero, and the fit resulted in zero values (Fig. 4, solid curve, and Table 3, fit (a)).

To find how accurately the model parameters can be determined form the given data, we have estimated errors in parameters using Monte Carlo simulations. Gaussian noise with the standard deviation corresponding to error bars of measured points was added to the values predicted

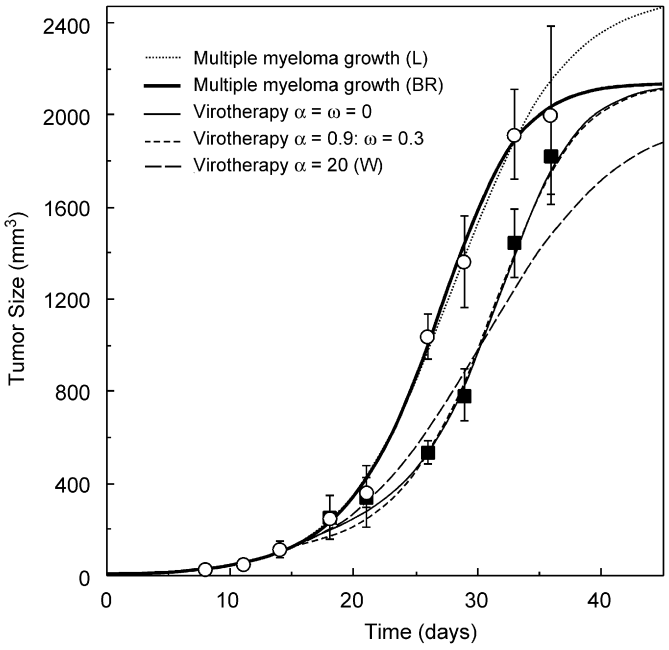

Fig. 4. Weighted least-squares fitting to growth data for multiple myeloma in SCID mice (Dingli et al., 2004). Error bars with circles denote data for untreated tumor and with squares for tumor under virotherapy. Untreated tumor data were fitted (Dingli et al., 2006a) using the generalized logistic model (6) with the result: $r = 0.2062134\,\text{day}^{-1}$, $K = 2139.258$, $\varepsilon = 1.648773$, (fit BR). The fit of untreated tumor data by the simple logistic model is also shown (fit L; see discussion in the text). When fitting to virotherapy data we assumed that the tumor size at the start of virotherapy on day 15 was given by the model curve for the untreated tumor, i.e., $y_0 = 126.237$, and the virus dose was $v_0 = 2$. The values of parameters obtained by fitting virotherapy data with model (10)–(12) are given in Table 3; fit (a) corresponds to thin solid curve and fit (d) to short-dash curve. Long dash curve corresponds to fit of virotherapy data with model (1) and (2) of Wodarz designated by W (see discussion in the text).

Table 3
Values of model rate constants (in day^{-1}) obtained by fitting to virotherapy data (see Fig. 4)

Fit	κ	δ	α	ω	ρ	χ^2
a	0.000959	0.512	0	0	0.215	1.0155
SD	0.000861	0.276	0.026	0.021	0.116	
b	0.000958	0.513	0.001	0.001	0.216	1.0175
c	0.000448	0.309	0.001	0.3	0.608	1.2839
d	0.000591	1.119	0.9	0.3	0.141	1.8489

Parameters $r, K, \varepsilon, y_0, v_0$ were as in Fig. 4. The last column presents the obtained χ^2. SD stands for standard deviations in parameters estimated for fit (a) (see text).

by the model. We fitted 400 simulated data, and obtained probability distributions for each parameter. It appeared that these distributions are bimodal, showing peaks at values comparable to those obtained by the fit to original data, and at much higher values. We have isolated unimodal distribution for lower values of parameters by neglecting all fits in which parameters κ and ρ were larger than five times the values of fit (a) (Table 3) and $\alpha < 1$. This criterion was satisfied for 128 parameter sets from which we obtained standard deviations displayed in Table 3. These deviations are quite large indicating that the existing six data points cannot provide accurate determination of the five parameters. In particular, α and ω appear to be the most difficult to accurately determine. It should be noted that in an ideal case when there is no noise, the fitting of the six model-predicted values yielded the original parameters quite accurately: $\kappa = 0.000958$, $\delta = 0.512$, $\alpha = 8 \times 10^{-11}$, $\omega = 6 \times 10^{-6}$, $\rho = 0.215$.

In terms of underlying biology one cannot completely exclude production of free virus and its elimination corresponding to $\alpha = \omega = 0$. However, some in vivo experiments (Peng et al., 2002a, 2006) suggest that the free virus population is not detectable, so one can infer that α is very small. On the other hand some in vitro experiments suggest that approximately $\frac{1}{3}$ of virus particles are inactivated per day (Whistler et al., 1996). This would indicate that $\omega \approx 0.3\,\text{day}^{-1}$. With that in mind, we have fitted data with various lower limits for allowable values of α and ω. Thus, for example, when we chose the lower limits $\alpha = 0.9\,\text{day}^{-1}$, $\omega = 0.3\,\text{day}^{-1}$ in the range of allowable parameter values, the minimization yielded those lower limits. The corresponding best-fit curve passes through error bars of data points and can possibly be considered consistent with data, although χ^2 is larger (see Table 3, fit (d), and the corresponding dashed curve in Fig. 4). When $\alpha > 0.9\,\text{day}^{-1}$ and $\omega = 0.3\,\text{day}^{-1}$ the best-fit curve no longer passes through the error bars, and we can consider those fits inconsistent with data. Fit (b) in Table 3 with small α and ω yields a curve that is within thickness of the line in Fig. 4 indistinguishable from the best-fit curve corresponding to fit (a). In fit (c) χ^2 is somewhat larger than in fits (a) and (b), yet the corresponding curve (shown in Fig. 5) is barely distinguishable from the best-fit curve (fit (a), certainly less than the curve of fit (d)). In general, Table 3 reveals that changes in α and ω lead to relatively smaller changes in other parameters, at most 53% decrease in κ, at most 46% decrease or 119% increase in δ and at most 46% decrease or 183% increase in ρ.

To demonstrate the effect of $-\kappa y v$ term in (12) we used parameters from Table 3 (fits (b)–(d)) and obtained growth curves for a model in which this term is omitted. They are depicted in Fig. 5 and compared with virotherapy data and acceptable fit (c) based on the full model (10)–(12). The effect is dramatic for small values of α and ω, as one can expect. For $\omega = 0.3\,\text{day}^{-1}$ and small values of α the effect is less pronounced.

Our model (10)–(12) fits the virotherapy data considerably better than the model (1) and (2) proposed by Wodarz (2001) (compare solid and dashed curves with the curve designated by W), Fig. 4. There are five free parameters: $d, \beta, s, a, x(0)$ in model (1) and (2). Parameters $\bar{r}$ and C were determined by fitting the logistic model to growth data of undisturbed tumor (Fig. 4, dotted curve designated by L). The fit to virotherapy data by (1) and (2) can be improved if the value for infected cell death rate is allowed to be

larger than $20\,\text{day}^{-1}$ which is the value allowed and retrieved for the fit in Fig. 4. This is already an unrealistic rate, equivalent to 99.3% of infected cells dying in 4 h. Interestingly, in this fit the value for s was nearly zero (see legend of Fig. 4), possibly indicating that infected cells do not proliferate.

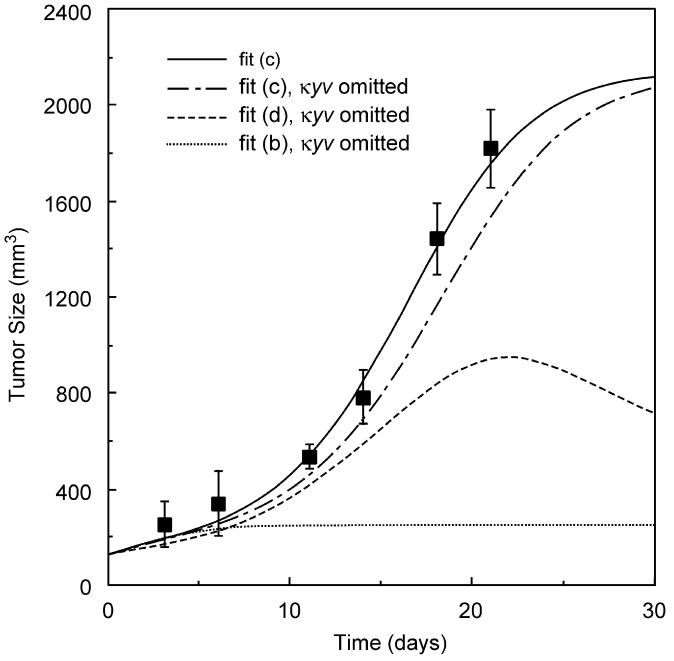

Fig. 5. The effects of κyv term in Eq. (12) of the model. Here the time zero is the beginning of virotherapy. Virotherapy data are well fitted by the solid curve corresponding to fit (c) of Table 3. The effect of omitting κyv for this fit is represented by the dot-dash curve. Other (still acceptable) fits of Table 3 are even more drastically influenced by the elimination of the term κyv.

Models (3)–(5) and (7)–(9) are deficient, as discussed in Section 2. Therefore, even if these models could fit the available virotherapy data (cf. Dingli et al., 2006a) well, they cannot be considered an adequate description of virotherapy.

5. Simulating successful therapy and oscillatory tumors

For parameters in Table 3, the model predicts therapy failure (equilibrium 2). Therefore, the question arises would the model predict a cure if the initial virus dose v_0 is increased. While this is possible theoretically, Figs. 2 and 3 suggest that v_0 has to be increased beyond levels that are reachable in practice. Thus, in the first part of this section we explore changes in the rate constants of the model which can result in a successful therapy with realistic levels of the initial virus dose. With modern gene therapy approaches it is possible to modify viruses that have different growth kinetics or cytopathic effects and one can use viruses in combination with chemotherapy to alter tumor growth rates. Therefore, it is reasonable to search for model parameters that yield tumor eradication within the lifetime of a mouse. In Fig. 6 we illustrate some patterns of virotherapy that may emerge for combinations of model parameters different than those in Table 3.

We note that some combinations of parameters lead to oscillating and sometimes pulsating population sizes of both tumor and virus. The oscillatory solutions have both important dynamical and physiological ramifications. Thus, in the second part of this section we investigate

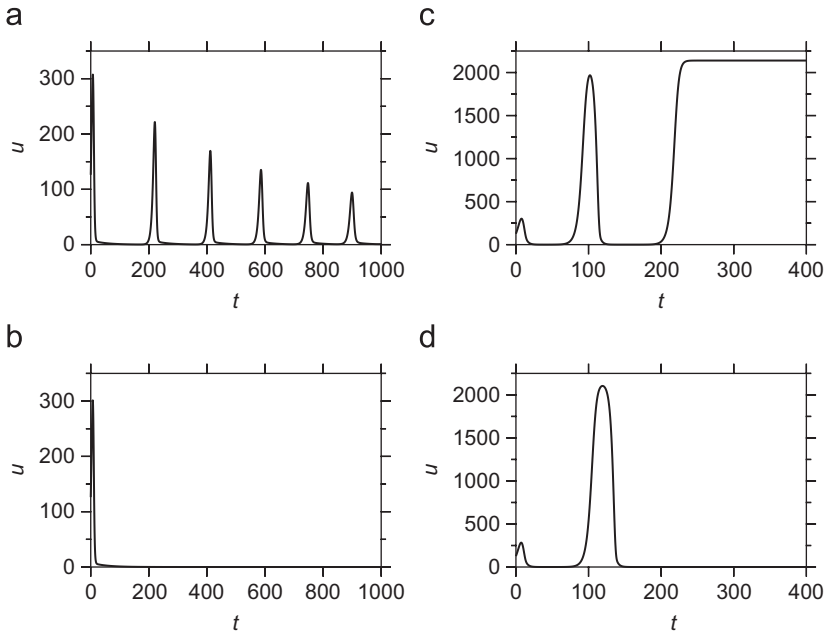

Fig. 6. Illustration of outcomes of virotherapy. Panel (a): average tumor burden is diminishing and $u(1000) = 1$. The values of model parameters are from Table 4, set d.1. Panel (b): the complete cure is achieved; parameters from Table 4, set d.2. Panel (c): therapy failure after oscillations with increasing amplitude; parameters $r, K, \varepsilon, y_0, v_0$ were as in Fig. 4, and $\kappa = 0.025$, $\delta = \omega = 0.3$, $\alpha = 0.6$, $\rho = 0.0177$. Panel (d): complete cure after two oscillations with increasing amplitude; parameters as in panel (c) except $\kappa = 0.0322$.

when oscillatory solutions occur, as well as the properties of the oscillations themselves, i.e., their amplitude and period.

5.1. Model predictions for successful therapy

When parameters of fit (b) in Table 3 are considered, the model requires that $v_0 > 311$ in order to obtain complete cure, i.e., that $u(t_e) = 10^{-6}$ is reached for some $t_e \leqslant 1000$. However, by changing some of the model parameters in Table 3 the model predicts operationally successful therapy $u(1000) \leqslant 1$ or complete cure, even for the experimentally applied dose $v_0 = 2$. If we consider fit (b), by increasing virus production rate to $\alpha = 1.3$, we can obtain success. However, during therapy the viral load reaches $v(1000) = 166$, which is not compatible with currently available data. By increasing the parameter ρ to 0.5, the viral load is reduced to 120, but this is still high. To obtain the results representing successful therapy or complete cure, while keeping viral load at more acceptable levels ($\leqslant 25$), one would have to decrease parameter δ. In Table 4 we list some combinations of values for parameters α, δ (and ρ in fit (b)) that yielded successful therapy or complete cure; other parameters were kept at values given in Table 3.

Fig. 6 panels (a) and (b) show total tumor burden $u(t)$ for parameters d.1 and d.2 of Table 4, respectively. Panel (a) shows damped pulsating oscillations with slightly increasing minima, but $u(1000) = 1$. The therapy can be deemed successful in a sense that during the lifetime of the mouse, the tumor burden is under control showing an average decrease towards the equilibrium $x_3 + y_3 = 9.77$. If parameter α is slightly increased (set d.2 in (4)) complete cure is obtained at time $t_e = 758$ (see Fig. 6, panel (b)). This is due to rapid depletion of non-infected cells, reaching the value 10^{-6} at time $t = 72.6$. At that point, according to our model this population is considered extinct and its size is set to zero. Infected cells are still present, but according to Eq. (8), their number diminishes exponentially with rate δ until they reach 10^{-6} and are considered eliminated.

Tumor burden for parameters b.1 of Table 4 in essence shows the same dynamics as for parameters d.1 (Fig. 6), exhibiting damped oscillations around the equilibrium at $x_3 + y_3 = 0.797$ (not shown). However, the peaks are much lower and the tumor burden is well controlled. Besides damped pulsating oscillations, we also observed another oscillatory regime in which amplitude increases with each cycle. In the same time the minima are becoming lower. As a consequence we observe complete eradication (Fig. 6, panel (d)) when the minimum becomes lower than 10^{-6}. Without this threshold the solution of model equations would exhibit stable oscillations. In a similar way the oscillations with increasing amplitude may turn into the limit of carrying capacity (Fig. 6, panel (c)). This is a result of the imposed threshold which is first reached by the infected population at time $t = 187.6$.

The oscillating nature of considered solutions may have important biological ramifications: As noted above, in the time between pulsations the tumor may reach a very small size. At the extreme, it may be so small that the tumor size is less than one cell and therefore considered eradicated. On the other hand, if $u(t) < 1$ then the tumor is undetectable, and the animal may erroneously be considered to be cured when, in fact, another large tumor spike is imminent. However, it is possible that additional therapies administered while the tumor is small may allow successful eradication of the disease.

Table 4
Model parameters yielding operationally successful therapy (sets b.1 and d.1) or complete cure (sets b.2 and d.2)

Set	κ	δ	α	ω	ρ	$u(1000)$	t_e
b.1	0.0009575	0.015	0.053	0.001	0.5	0.99	
b.2	0.0009575	0.015	0.25	0.001	0.5	0	952.8
d.1	0.0005911	0.021	1.3	0.3	0.1411	1.00	
d.2	0.0005911	0.021	1.4	0.3	0.1411	0	758

Designations b.1, b.2 and d.1, d.2 correspond to fits (b) and (d) in Table 3, respectively. Parameters $r, K, \varepsilon, y_0, v_0$ were as in Fig. 4. t_e is a time when tumor can be considered eradicated (see text).

5.2. Oscillations and Hopf bifurcation

The potential significance of the oscillatory solutions and their timing in determining therapy strategies motivates us to investigate the properties of the oscillatory solutions in more detail. At the end of Section 3.2 we noted that equilibrium 3, corresponding to partial therapeutic success, can become unstable via a Hopf bifurcation. The oscillations of the tumor and virus populations that appear are analogous to predator–prey type population models (Bruaer and Castillo-Chavez, 2000) with the virus playing the role of the predator and the tumor cells being the prey. In the remainder of this section we numerically determine the parameter values that give the Hopf bifurcation and explore the oscillatory solutions that occur both before and after the bifurcation using the software package XPPAUT (Ermantrout, 2002).

Figs. 7 and 8 show the oscillations in the total tumor size $u = y + x$ for parameter values such that the Hopf bifurcation has occurred. Notice that in Fig. 8 the scale for u is logarithmic such that the forms of the time series indicate pulsating oscillations. These oscillations require a very large α and perhaps apply for lytic viruses such as adenovirus or vesicular stomatitis virus (VSV). The rate of virus elimination also determines the reference value around which the oscillations occur, as well as the frequency and depth of the oscillations. As expected, slower elimination of the virus is associated with a smaller average value of $u(t)$ and therefore a smaller average tumor burden.

While the parameter values required to exhibit self-sustained oscillations are outside the ranges suggested by fitting experimental data (see Section 4), their physiological importance warrant further investigation, especially with

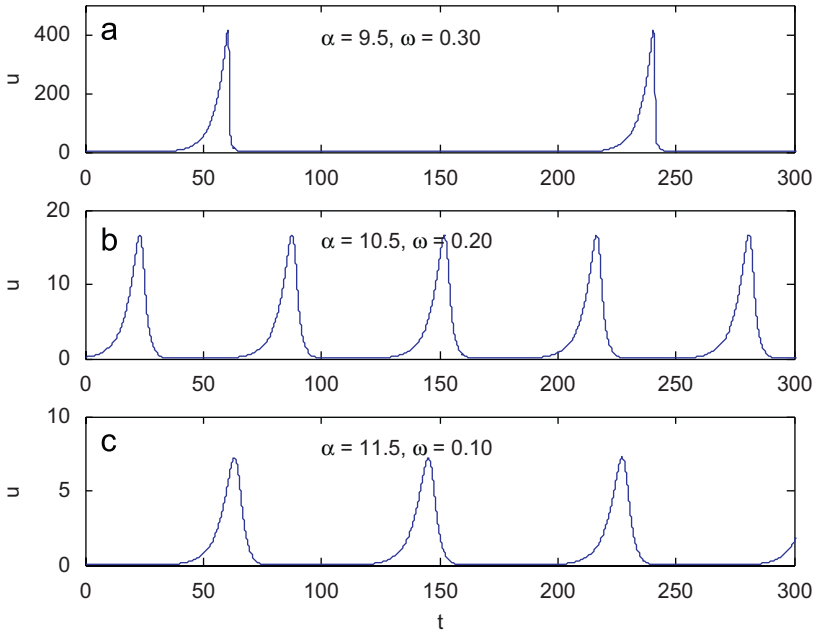

Fig. 7. Pulsating oscillations for different combinations of α and ω. Fixed parameter values are $r = 0.206$, $K = 2139, \varepsilon = 1.649$, $\kappa = 0.01$, $\rho = 0.21$ and $\delta = 0.51$, corresponding to Fig. 10a.

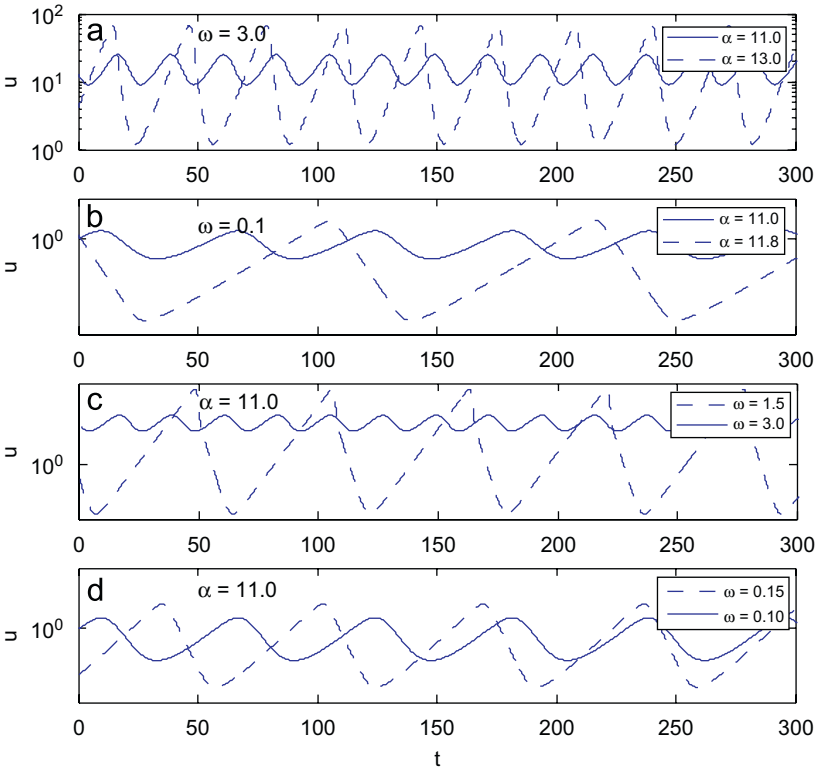

Fig. 8. Time series for different values of α with ω fixed at (a) $\omega = 3.0$, (b) $\omega = 0.1$. (c) and (d) Time series for different values of ω with $\alpha = 11$. Fixed parameter values are the same as in Fig. 7.

other vector systems that include cell lysis during their life cycle. In Fig. 9 we plot the neutral stability curves for different combinations of the parameters. The neutral stability curve indicates the parameter values where the linear-stability analysis of equilibrium 3 shows that a pair of complex-conjugate eigenvalues crosses the imaginary axis with real parts equal to zero. For example, in Fig. 9a, for a fixed value of ω and for low values of α the partial-success equilibrium 3 is stable. As α is increased, the neutral stability curve indicates the critical value of $\alpha = \alpha_H$ for the

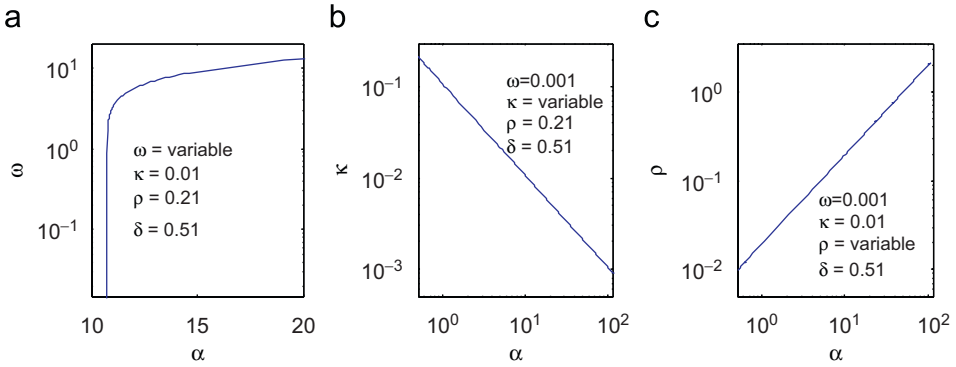

Fig. 9. Neutral stability curves that define the critical values of the parameters that lead to a Hopf bifurcation. For α less than the critical value there are no oscillations and the steady state (y_3, x_3, v_3) is stable. For α greater than the critical value, the tumor size and the virus population exhibit oscillations. Notice that the parameter values in (a) are essentially those of Table 3(a). Other parameter values are $r = 0.206$, $K = 2139$, $\varepsilon = 1.649$.

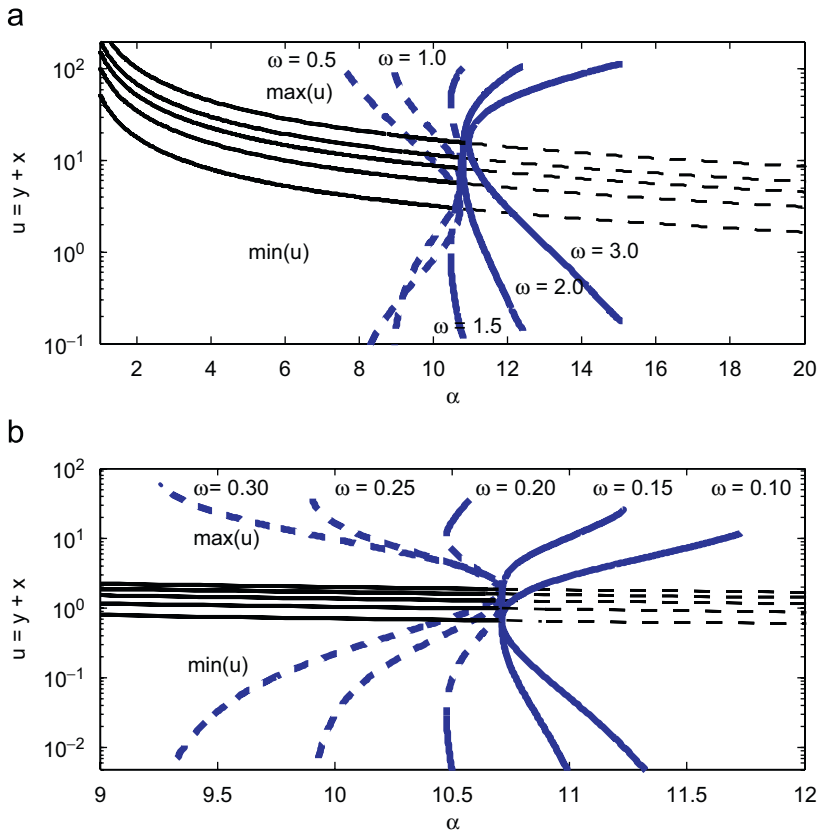

Fig. 10. Bifurcation diagrams that show the maximum and minimum values of the oscillations in the tumor size u, as a function of α for different values of ω. The thin solid (dashed) line represents the stable (unstable) steady state (y_3, x_3, v_3). The thick dashed curves indicate the amplitude of unstable oscillatory solutions, while the red curves indicate the amplitude of the stable oscillations. Parameter values are those of Fig. 9a.

Hopf bifurcation. For α to the right of the neutral stability curve ($\alpha > \alpha_H$), equilibrium 3 is unstable and the system exhibits oscillations. Figs. 9a and b are similar in that for κ and ρ fixed and for low values of α equilibrium 3 is stable, while for larger values oscillations are exhibited. In each case we observe that only large rates of virion generation lead to sustained oscillations in the population sizes.

To better understand the affect of the virus on the dynamics of the cancer, we have performed a numerical bifurcation analysis using α and ω, the virus production and elimination rates, respectively, as control parameters. Fig. 10 shows bifurcation diagrams for different values of ω as α is increased. The thin, solid curve indicates the stable steady-state value of $u_3 = y_3 + x_3$, which decreases for increasing α. The thin, dashed curve indicates the values of α where u_3 is unstable. The thick, solid and dashed curves indicate stable and unstable oscillatory solutions, respectively. For example, in Fig. 10a for $\omega = 3.0$ the amplitude

of the oscillations in u_3 is described by the right-most thick, solid curve. The Hopf bifurcation curve is supercritical so that there is a smooth increase in the amplitude of the oscillations as α is increased. However, the increase in the amplitude with α occurs quickly, and for only an $O(1)$ increase of α beyond the Hopf bifurcation point, e.g., from $\alpha_H \approx 10.7$ to $\alpha = 14$, the oscillations are pulsating with maximum values in u of $O(10^2)$, while the minima are $O(10^{-1})$.

We mention that the pulsating solutions pose numerical difficulties for the continuation package we use Ermantrout (2002). This is because the pulses change rapidly over a very short time interval, while during the time between pulses the solution is very small. Both of these properties require very strict accuracy tolerances. Thus, in general, the fact that the bifurcation curves have not been computed further is due to the solver not being able to accurately track the solution.

As ω is decreased the bifurcation curve goes from supercritical to subcritical. For example, when $\omega = 1.5$, the branch of oscillatory solutions that emanates from the Hopf bifurcation bends backwards and is unstable. Thus, for α just greater than the critical value α_H, the solution will jump up the thick, solid curve and exhibit high-amplitude pulsating solutions (see Fig. 7c). For $\omega = 1.0$ and 0.5 the bifurcation is even more subcritical in that the branch of periodic solutions bends backwards even farther. Again, as α is increased beyond α_H the system jumps up to very large-amplitude pulsating solutions.

Fig. 10b shows that subcritical Hopf bifurcations also occur for $\omega = 0.3$, 0.25 and 0.20. Whenever there is a subcritical bifurcation there is an interval in α of bistability between the stable steady state and stable oscillations. The upper limit of this interval is defined by the Hopf bifurcation point at α_H, beyond which the steady state is unstable. The lower limit is defined by the limit point on the branch of oscillatory solutions defined by where the thick, dashed curve becomes the thick, solid curve (see the cases when $\omega = 1.0$ and 2.0). Within the interval of bistability the final state of the system, either steady state or pulsating, is determine by the initial conditions. In Figs. 7a and b the initial conditions were chosen such that the system evolved to the very high-amplitude pulsating solution instead of the steady state.

In Figs. 8a and b we show time series for u for the cases $\omega = 3.0$ and 0.1, respectively. In each of these cases the bifurcation is supercritical. For $\omega = 0.3$ the oscillations become high-amplitude pulsations as α is increased. For $\omega = 0.1$ the oscillations also become pulsating as α is increased by the amplitudes are not as large.

Of particular note is that when $\omega = 0.1$ the period of the oscillations becomes very long. This is because for smaller ω, the virus population will persist for a longer time, given a number of tumor cells. Therefore, as ω is decreased, the total number of tumor cells u can be driven to a lower level, before a subsequent recurrent outbreak.

6. Concluding remarks

Tumor virotherapy is an exciting new approach for cancer treatment since many viruses preferentially infect and destroy tumor cells, either naturally or due to genetic engineering. While many tumors often become resistant to chemotherapy due to mutagenesis, viruses themselves can evolve rapidly in time and it is possible that tumor cells will not be able to become resistant to the oncolytic effect of the virus. The biological basis of this is the observation that often viruses usurp specific pathways that are required by the cancer cell for its survival. However, it is clear that tumor virotherapy is a highly non-linear process, and very sensitive to initial conditions. The outcomes are expected to be more variable in patients due to small changes in the rates that could emerge from the known genetic heterogeneity of tumors. In this context, mathematical models assist in the understanding of the dynamic interactions between populations and suggest mechanisms to optimize therapy by limiting the possible scenarios and guide further experimental work.

The utility of models is critically dependent on how faithfully they capture the salient biological features of the system. The current work highlights this point very clearly by a comparison between our model and those proposed by Wodarz (2001, 2003) and Wodarz and Komarova (2005). His model (Wodarz, 2001) implicitly requires a virus to integrate into the genome of the target cells, a feature of retro/lentiviruses and adeno-associated viruses but this is not typical of the viruses currently undergoing studies for patients with cancer. Our model is more general; it can accommodate infection induced cell-to-cell fusion ($\rho > 0$) and lytic viruses such as adenovirus and VSV that destroy cells by lysis with the release of many virus particles, without inducing cell-to-cell fusion ($\rho = 0$). Moreover, to our knowledge, no prior model has considered the decrease of the free virus population due to infection of the cells and the term κyv is conspicuously absent in all. However, proper accounting of the populations is essential as our results in Fig. 5 show.

The model presented is parsimonious in the sense that each biologically important factor is presented just with one simple rate term. The rate of MV production in vivo appears to be small and the cytopathic effect is mainly due to cell-to-cell fusion of virus infected cells with the surrounding cells to form syncytia that ultimately die. One can consider a more complex model where it is assumed that infected cells interact with surrounding cells and form syncytia with probability p, while with probability $1-p$ the infected cell transfers virus to the neighboring cell but the fusion does not occur. This would introduce an additional rate term of the form $(1-p)\rho xy$ in Eq. (11). We have fitted data by such a model with the result that the estimated p was very nearly 1. This suggested that the probability that infected cells pass on the virus to neighboring cells without fusion is very small, if it happens at all, and therefore the term $(1-p)\rho xy$ can be neglected.

Our simulations suggest that weakly cytopathic viruses (δ small) provide more tumor cytoreduction than viruses that destroy cells rapidly. Also we found that oscillations in all populations considered can follow three patterns organized around Hopf bifurcation. If α is sufficiently large the dynamics is characterized by a stable limit cycle. For smaller α we have observed either damped oscillations limiting to equilibrium 3 (Table 2) or pulsating oscillations of increasing amplitude that can lead to equilibrium 2 (Fig. 6, panel (c)). In the course of such oscillations the minima can reach the defined criteria for cure (Fig. 6, panel (d)). Perhaps the concept of an oscillating tumor may appear unusual to some of the readers but in fact, such behavior has been observed in various malignant and "benign" hematopoietic disorders either spontaneously or in response to therapy. The possibility of oscillatory behavior in response to tumor virotherapy should caution that tumors may re-surge even after they may appear to be cured and hence long term observation will be necessary before cure can be declared.

Acknowledgments

This research has been supported by NIH Grants CA-100634 (S.J. Russel and Ž. Bajzer), CA15083 and Mayo-Santulli Fund (Ž. Bajzer), and NSF Grant NSF-0604429 (K. Josić). We thank Mr. Ken Peters for assisting in preparation of Figs. 1, 4 and 5.

References

Anderson, B.D., Nakamura, T., Russell, S.J., Peng, K.W., 2004. High cd46 receptor density determines preferential killing of tumor cells by oncolytic measles virus. Cancer Res. 64 (14), 4919–4926.

Bajzer, Ž., Marušić, M., Vuk-Pavlović, S., 1996. Conceptual frameworks for mathematical modeling of tumor growth dynamics. Math. Comput. Modelling 23, 31–46.

Bajzer, Ž., Vuk-Pavlović, S., Huzak, M., 1997. Mathematical modeling of tumor growth kinetics. In: Adam, J., Bellomo, N. (Eds.), A Survey of Models for Tumor-immune System Dynamics. Birkhäuser, New York, NY, pp. 89–133 (Chapter 3).

Bruaer, F., Castillo-Chavez, C., 2000. Mathematical Models in Population Biology and Epidemiology. Springer, New York, NY.

Byrne, H.M., 2003. Modelling avascular tumour growth. In: Preziosi, L. (Ed.), Cancer Modelling and Simulation. CRC Press, Boca Raton, FL, pp. 75–120 (Chapter 4).

Cameron, D.A., Ritchie, A.A., Miller, W.R., 2001. The relative importance of proliferation and cell death in breast cancer growth and response to tamoxifen. Eur. J. Cancer 37 (12), 1545–1553.

Chignola, R., Schenetti, A., Andrighetto, G., Chiesa, E., Foroni, R., Sartoris, S., Tridente, G., Liberati, D., 2000. Forecasting the growth of multicell tumour spheroids: implications for the dynamic growth of solid tumours. Cell Prolif. 33 (4), 219–229.

Dingli, D., Peng, K.W., Harvey, M.E., Greipp, P.R., O'Connor, M.K., Cattaneo, R., Morris, J.C., Russell, S.J., 2004. Image-guided radiovirotherapy for multiple myeloma using a recombinant measles virus expressing the thyroidal sodium iodide symporter. Blood 103 (5), 1641–1646.

Dingli, D., Cascino, M.D., Josić, K., Russell, S.J., Bajzer, Ž., 2006a. Mathematical modeling of cancer radiovirotherapy. Math. Biosci. 199 (1), 55–78.

Dingli, D., Kemp, B.J., O'Connor, M.K., Morris, J.C., Russell, S.J., Lowe, V.J., 2006b. Combined I-124 positron emission tomography/computed tomography imaging of nis gene expression in animal models of stably transfected and intravenously transfected tumor. Mol. Imaging Biol. 8 (1), 16–23, (1536–1632).

Ermantrout, B., 2002. Simulating, Analyzing, and Animating Dynamical Systems: A Guide to Xppaut for Researchers and Students. Society for Industrial and Applied Mathematics, Philadelphia, PA.

Friedman, A., Tian, J., Fulci, G., Chiocca, E., Wang, J., 2006. Glioma virotherapy: effects of innate immune suppression and increased viral replication capacity. Cancer Res. 66, 2314–2319.

Grote, D., Russell, S.J., Cornu, T.I., Cattaneo, R., Vile, R., Poland, G.A., Fielding, A.K., 2001. Live attenuated measles virus induces regression of human lymphoma xenografts in immunodeficient mice. Blood 97 (12), 3746–3754.

Hadac, E.M., Peng, K.W., Nakamura, T., Russell, S.J., 2004. Reengineering paramyxovirus tropism. Virology 329 (2), 217–225.

Heaney, J., Barrett, T., Cosby, S.L., 2002. Inhibition of in vitro leukocyte proliferation by morbilliviruses. J. Virol. 76 (7), 3579–3584.

Kirn, D., Martuza, R.L., Zwiebel, J., 2001. Replication-selective virotherapy for cancer: biological principles, risk management and future directions. Nat. Med. 7 (7), 781–787.

Marušić, M., Bajzer, Ž., Vuk-Pavlović, S., Freyer, J.P., 1994. Tumor growth in vivo and as multicellular spheroids compared by mathematical models. Bull. Math. Biol. 56 (4), 617–631.

McDonald, C.J., Erlichman, C., Ingle, J.N., Rosales, G.A., Allen, C., Greiner, S.M., Harvey, M.E., Zollman, P.J., Russell, S.J., Galanis, E., 2006. A measles virus vaccine strain derivative as a novel oncolytic agent against breast cancer. Breast Cancer Res. Treat. 99 (2), 177–184.

Nakamura, T., Peng, K.W., Vongpunsawad, S., Harvey, M., Mizuguchi, H., Hayakawa, T., Cattaneo, R., Russell, S.J., 2004. Antibody-targeted cell fusion. Nat. Biotechnol. 22 (3), 331–336.

Nakamura, T., Peng, K.W., Harvey, M., Greiner, S., Lorimer, I.A., James, C.D., Russell, S.J., 2005. Rescue and propagation of fully retargeted oncolytic measles viruses. Nat. Biotechnol. 23 (2), 209–214.

Nemunaitis, J., Khuri, F., Ganly, I., Arseneau, J., Posner, M., Vokes, E., Kuhn, J., McCarty, T., Landers, S., Blackburn, A., Romel, L., Randlev, B., Kaye, S., Kirn, D., 2001. Phase ii trial of intratumoral administration of onyx-015, a replication-selective adenovirus, in patients with refractory head and neck cancer. J. Clin. Oncol. 19 (2), 289–298.

Offord, C., Bajzer, Ž., 2006. A hybrid global optimization algorithm involving simplex and inductive search. Lecture Notes in Computer Science, vol. 2074. Springer, Berlin, pp. 680–688.

Ong, H.T., Timm, M.M., Greipp, P.R., Witzig, T.E., Dispenzieri, A., Russell, S.J., Peng, K.W., 2006. Oncolytic measles virus targets high cd46 expression on multiple myeloma cells. Exp. Hematol. 34 (6), 713–720.

Pecora, A.L., Rizvi, N., Cohen, G.I., Meropol, N.J., Sterman, D., Marshall, J.L., Goldberg, S., Gross, P., O'Neil, J.D., Groene, W.S., Roberts, M.S., Rabin, H., Bamat, M.K., Lorence, R.M., 2002. Phase i trial of intravenous administration of pv701, an oncolytic virus, in patients with advanced solid cancers. J. Clin. Oncol. 20 (9), 2251–2266.

Peng, K.W., Ahmann, G.J., Pham, L., Greipp, P.R., Cattaneo, R., Russell, S.J., 2001. Systemic therapy of myeloma xenografts by an attenuated measles virus. Blood 98 (7), 2002–2007.

Peng, K.W., Facteau, S., Wegman, T., O'Kane, D., Russell, S.J., 2002a. Non-invasive in vivo monitoring of trackable viruses expressing soluble marker peptides. Nat. Med. 8 (5), 527–531.

Peng, K.W., TenEyck, C.J., Galanis, E., Kalli, K.R., Hartmann, L.C., Russell, S.J., 2002b. Intraperitoneal therapy of ovarian cancer using an engineered measles virus. Cancer Res. 62 (16), 4656–4662.

Peng, K.W., Hadac, E.M., Anderson, B.D., Myers, R., Harvey, M., Greiner, S.M., Soeffker, D., Federspiel, M.J., Russell, S.J., 2006. Pharmacokinetics of oncolytic measles virotherapy: eventual equilibrium between virus and tumor in an ovarian cancer xenograft model. Cancer Gene Ther. 13 (8), 732–738.

Phuong, L.K., Allen, C., Peng, K.W., Giannini, C., Greiner, S., TenEyck, C.J., Mishra, P.K., Macura, S.I., Russell, S.J., Galanis, E.C., 2003. Use of a vaccine strain of measles virus genetically engineered to produce carcinoembryonic antigen as a novel therapeutic agent against glioblastoma multiforme. Cancer Res. 63 (10), 2462–2469.

Reid, T., Galanis, E., Abbruzzese, J., Sze, D., Andrews, J., Romel, L., Hatfield, M., Rubin, J., Kirn, D., 2001. Intra-arterial administration of a replication-selective adenovirus (dl1520) in patients with colorectal carcinoma metastatic to the liver: a phase i trial. Gene Ther. 8 (21), 1618–1626.

Reid, T., Galanis, E., Abbruzzese, J., Sze, D., Wein, L.M., Andrews, J., Randlev, B., Heise, C., Uprichard, M., Hatfield, M., Rome, L., Rubin, J., Kirn, D., 2002. Hepatic arterial infusion of a replication-selective oncolytic adenovirus (dl1520): phase ii viral, immunologic, and clinical endpoints. Cancer Res. 62 (21), 6070–6079.

Russell, S.J., 2002. RNA viruses as virotherapy agents. Cancer Gene Ther. 9 (12), 961–966.

Schneider, U., von Messling, V., Devaux, P., Cattaneo, R., 2002. Efficiency of measles virus entry and dissemination through different receptors. J. Virol. 76 (15), 7460–7467.

Spratt, J.A., von Fournier, D., Spratt, J.S., Weber, E.E., 1993. Decelerating growth and human breast cancer. Cancer 71 (6), 2013–2019.

Tao, Y., Guo, Q., 2005. The competitive dynamics between tumor cells, a replication-competent virus and an immune response. J. Math. Biol. 51 (1), 37–74.

Wein, L.M., Wu, J.T., Kirn, D.H., 2003. Validation and analysis of a mathematical model of a replication-competent oncolytic virus for cancer treatment: implications for virus design and delivery. Cancer Res. 63 (6), 1317–1324.

Whistler, T., Bellini, W.J., Rota, P.A., 1996. Generation of defective interfering particles by two vaccine strains of measles virus. Virology 220 (2), 480–484.

Wodarz, D., 2001. Viruses as antitumor weapons: defining conditions for tumor remission. Cancer Res. 61 (8), 3501–3507.

Wodarz, D., 2003. Gene therapy for killing p53-negative cancer cells: use of replicating versus nonreplicating agents. Hum. Gene Ther. 14 (2), 153–159.

Wodarz, D., Komarova, N., 2005. Computational Biology of Cancer: Lecture Notes and Mathematical Modeling. World Scientific Publishing Company, Hackensack, NJ.

Wu, J.T., Byrne, H.M., Kirn, D.H., Wein, L.M., 2001. Modeling and analysis of a virus that replicates selectively in tumor cells. Bull. Math. Biol. 63 (4), 731–768.

Wu, J.T., Kirn, D.H., Wein, L.M., 2004. Analysis of a three-way race between tumor growth, a replication-competent virus and an immune response. Bull. Math. Biol. 66 (4), 605–625.